A Synopsis of the thesis entitled

"Synthesis, Spectral Characterization and Structural Analysis of Transition Metal Complexes Containing Acyl Pyrazolone Ligands and their Applications"

To be submitted to

The Maharaja Sayajirao University of Baroda

For the Degree of

DOCTOR OF PHILOSOPHY

In Chemistry

By

Barad Sapnaben Vishnubhai

Under the Guidance of

Dr. R. N. Jadeja

Department of Chemistry,

Faculty of Science,

The Maharaja Sayajirao University of Baroda

VADODARA- 390002,

GUJARAT

2024

Synopsis of the Thesis

To be submitted to The Maharaja Sayajirao University of Baroda for the degree of DOCTOR OF PHILOSOPHY in Chemistry

Title of the Thesis: "Synthesis, Spectral Characterization and Structural Analysis of Transition Metal Complexes Containing Acyl Pyrazolone Ligands and their Applications"

Name of the Student: Barad Sapnaben Vishnubhai

Name of the Supervisor: Dr. R. N. Jadeja

Department: Chemistry

Faculty: Science, The Maharaja Sayajirao University of Baroda

Registration number: FOS/2301

Date of registration: 27th October 2021

Barad Sapnaben Vishnubhai
Research Scholar

Dr. R. N. Jadeja
Research Guide

Department of Chemistry,
Faculty of Science,
The Maharaja Sayajirao University of Baroda
Vadodara.-390002. GUJARAT- INDIA.

The synopsis contains the synthesis and characterization of heterocyclic Acylpyrazolone ligands, Copper(II) and Nickel(II) complexes based on Acylpyrazolone ligands. Characterization was done using all available techniques such as IR, NMR, Mass, TGA, Uv-Vis, Single crystal X-ray diffraction, Powder XRD, CV, ESR, Magnetic study etc. In-vitro anticancer analysis, Cytotoxicity assay of the synthesized Copper(II) complexes has been done.

The thesis will be presented in the form of the following chapters:

Chapter 1: Introduction of transition metal complexes containing a derivative of pyrazolone ligands and their coordination chemistry

1 Introduction

Transition metal chemistry and their characteristics

It has an extensive history of coordination compounds to develop coordinate bonds using donor atoms including sulphur, oxygen, and nitrogen [1]. Metal ions play major functions in human beings. The deficiency of some metal ions can result to disease. The biological systems and the role of metal ions have been recognized for a long period. Transition metals have so many distinctive qualities such as different coordination modes, and different oxidation states. Their interactions with negatively charged molecules and reactivity towards organic substrates increase their importance [2].

Importance of Nickel and Copper metals

In many fields of material chemistry, nickel is an essential metal and is used in modern metallurgies in a broad variety of metallurgical processes. Being more stable than Nickel(0), Nickel(I), Nickel(III) and Nickel(IV). The most prevalent geometrical forms of Nickel (II) are octahedral and square planar [3]. With its d9 electron system, Cu is a fascinating metal that shows off a variety of coordination compounds, especially those with coordination numbers four, five, and six. Copper exists in nature as Cu^{2+}. Copper complexes are renowned for their efficiency in the treatment of cancer because of their cytotoxic effect on tumour cells.

A pyrazolone chemistry

Pyrazolone can be viewed as a derivative of pyrazole possessing an additional carbonyl (C=O) group. Pyrazolone is a Five-membered heterocycle that is particularly helpful in the synthesis of organic compounds. At the end of the 19th century, an acylpyrazolone was first synthesized. By 1959, Jensen had developed a useful technique to synthesized 1-phenyl-3-methyl-4-acylpyrazol-5-ones. Acylpyrazolone is a well-known derivative of pyrazolone, an interesting class of β-diketones containing a pyrazole fused to a chelating arm and serve a special role in the field of drug discovery [4].

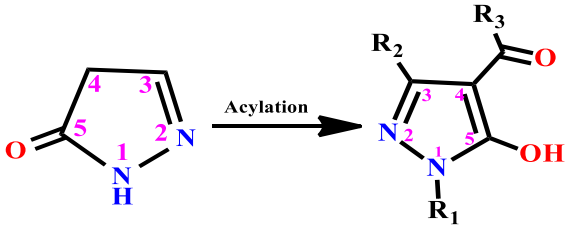

Fig.1.1 Synthesis of acylpyrazolone ligand

Transition metals complexes based on Acylpyrazolone ligand and their biological importance

When it comes to biological and pharmacological uses, copper metal complexes containing specific bioactive ligands may work better than their free form. The advances in bioinorganic chemistry provide better opportunities to use metal complexes as therapeutic agents. Therefore metal based drugs will surely take a key part of drug development. More study is being done on these complexes because of their significance in bioinorganic chemistry. Abnormal levels of metal ions are linked to several pathological illnesses and harmful side effects, including cancer. And Cu(II) complexes are thought to be the most effective hence, we have selected the biocompatible metal Copper for the study. Nickel metal has also been taken for the study [2].

Chapter 2: Synthesis, Crystal Features and Characterization of a series of acylpyrazolone ligands: Computational analysis

2 Experimental work

2.1 Synthetic route of HL^{I}, HL^{II}, HL^{III} ligands

All three ligands were prepared by the following method suggested by jenson. In 3 necked R.B flask, pyrazolone and 1,4 dioxane (40 ml) were added along with 2 eq amount of Calcium hydroxide followed by dropwise addition of 1 eq amount of 2,4-dichloro benzoyl chloride (R^3). 2M hydrochloric acid(200ml) was added to the reaction mixture. The obtained product was recrystallized in Rectified spirit. p-chloro benzoyl chloride was used as a R^3

to synthesized HL^{IV}, HL^{V}, HL^{VI} ligands [5] while 3,5-dimethyl benzoyl chloride (R^3) was used to synthesized HL^{VII}, HL^{VIII} ligands[6][7].

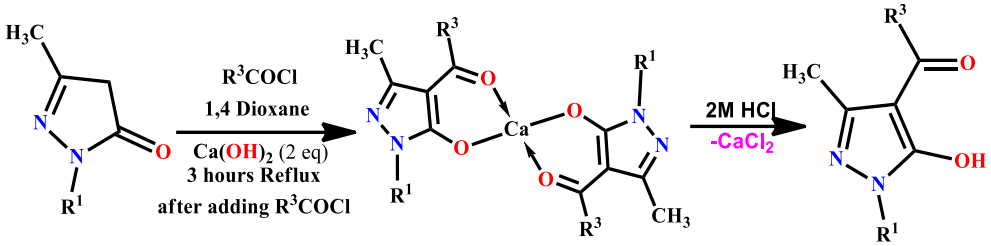

Fig.2.1. Synthesis of acylpyrazolone ligands

R^1= HL^I ligand, R^1= HL^{II} ligand, R^1= HL^{III} ligand

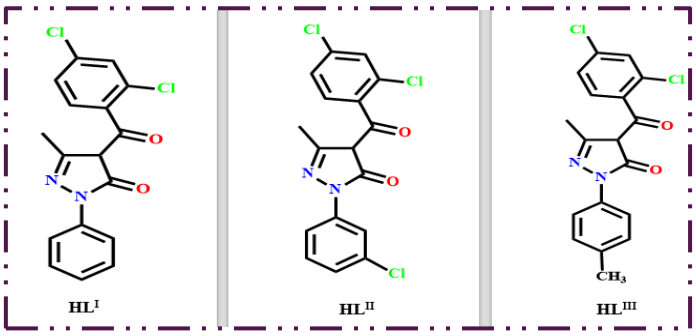

HL^I ligand: Light orange, yield:85%, M.P: 128°C, Molecular formula: $C_{17}H_{12}Cl_2N_2O_2$, M.W: 347.20, **FTIR (KBr, cm^{-1}):**1627($\nu_{C=O}$ of pyrazolone), 1587($\nu_{C=O}$ of benzoyl),1501($\nu_{C=N}$). NMR:**^{1}H NMR δ-ppm (400 MHz, $CDCl_3$):** 2.195 (s, 3H, CH_3(pyz)), 7.3–7.8 (m, Ar-H of HL^I ligand), 13C NMR δ-ppm (100 MHz, CDCl3): 14.02 (pyrazolone CH3), 104.33 (pyrazolone ring-C)**.**

HL^{II} ligand: Brownish crystals, **yield:**86%, **M.P**: 135°C, **Molecular formula**:$C_{17}H_{11}Cl_3N_2O_2$, M.W: 381.64, **FTIR(KBr,cm^{-1}):** 1594($\nu_{C=O}$ of 2,4 dichloro benzoyl), 1482(cyclic $\nu_{C=N}$), 1062 (C–H in plane deformation), **^{1}H NMR δ-ppm (400 MHz, CDCl3)**: d ppm:1.89 (s, 3H, Pyrazolone C-CH3), 7.3–7.9 (m, Ar-H of HL^{II} ligand).

HL^{III} ligand: Orange-brown: yield:86%, **M.P**: 131°C, **Molecular formula:** $C_{18}H_{14}Cl_2N_2O_2$, M.W: 361.22, **FTIR(KBr,cm^{-1}):** 1668 ($\nu_{C=O}$ of pyrazolone), 1585($\nu_{C=O}$ of 2,4 dichloro benzoyl), 1472(cyclic $\nu_{C=N}$), 1253(C–H in plane deformation), **^{1}H NMR δ-ppm (400 MHz, CDCl3)**: d ppm:1.94 (s, 3H, Pyrazolone C-CH3), 7.4–7.7 (m, Aromatic-H of HL^{III} ligand).

2.2 Results and discussion

2.2.1. ^{1}H NMR spectroscopic Study

The ^{1}H NMR spectra of the synthesized HL^I, HL^{II}, HL^{III} ligands in $CDCl_3$ are in good agreement with the proposed structure.

2.2.2. FTIR spectral studies

Infrared spectra (4000-400 cm^{-1} KBr discs) of prepared complex was done on model Brucker alpha.

HL^I **HL^{II}**

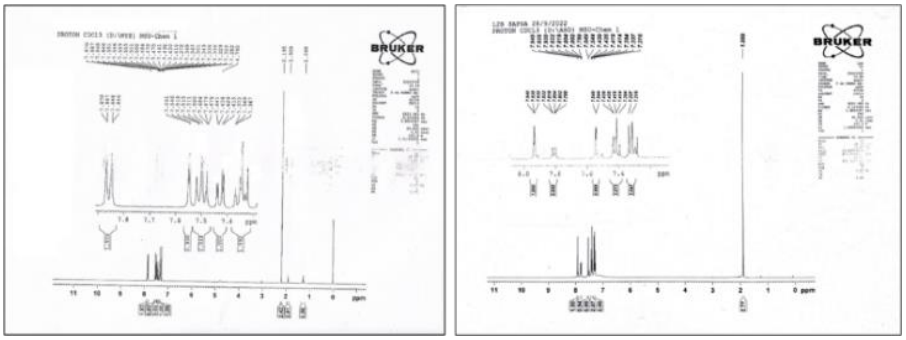

Fig.2.2. ^{1}H-NMR spectra of HL^I, HL^{II} ligands

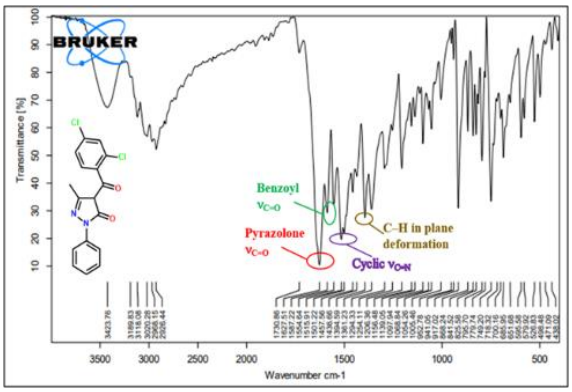

Fig.2.3. FTIR spectra of HL^{I} ligand

2.2.3. Single crystal X-ray diffraction study

Crystal structure of HL^{I}, HL^{II}, HL^{III} ligands were obtained in the form of keto, enol and keto having Triclinic crystal system with P -1 space group, Monoclinic crystal system with P2(1)/n' space group**,** Triclinic crystal system with P-1 space group respectively.

HL^{I}: Z= 2, α= 93.586(2)°, β= 90.901(2)°, γ= 105.568(2)°, a= 11.5502(3) Å, b= 11.5976(3)Å, c= 12.1851(3)Å

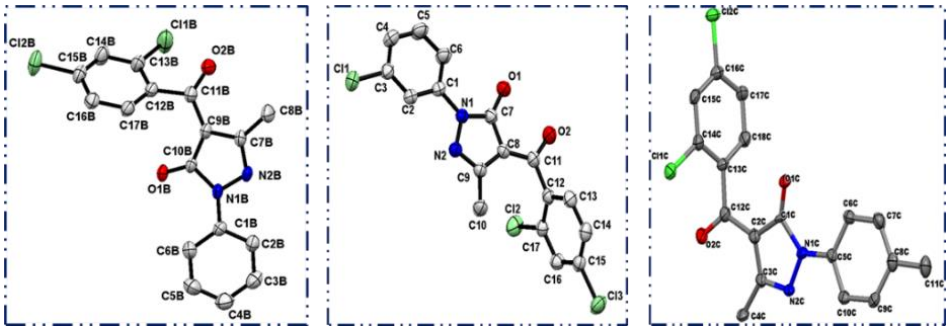

Fig.2.4. ORTEP diagram of HL^{I}, HL^{II}, HL^{III} ligands with 50% probability level respectively

2.2.4. Computational analysis employing DFT

B3LYP/6-31G level basis set was used to compute the optimized geometry of ligands with energy value -49.934 keV, -62.440 keV and -51.004 keV for HL^{I}, HL^{II}, HL^{III} ligands accordingly. HOMO-LUMO energies are crucial in determining a wide range of chemical interactions. The distribution of frontier orbital can be used to analyse active sites and reactivity of complex. HOMO-LUMO gives an idea about molecule's nature.

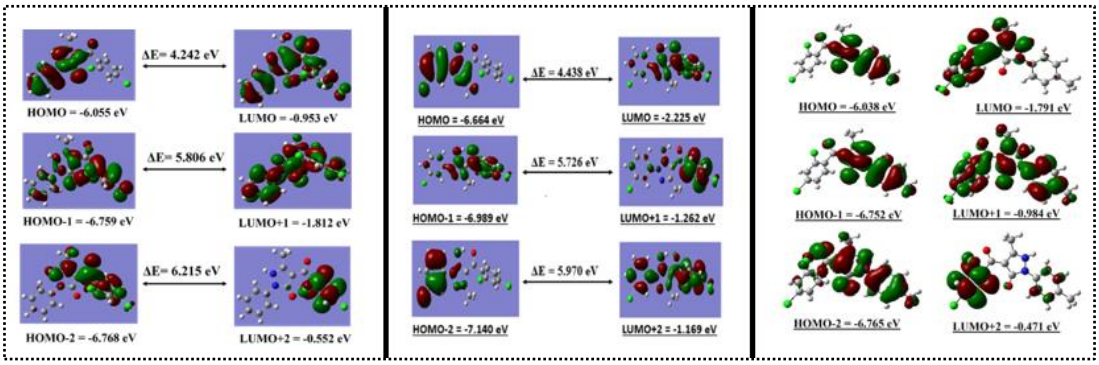

Fig.2.5. HOMO-LUMO molecular diagram of HL^{I}, HL^{II}, HL^{III} ligands

2.2.5. Hirshfeld surface analysis

To learn more about how molecules interact in crystal formations, we have employed Hirshfeld surfaces analysis. This study has provided a thorough description of an immediate surroundings of the molecule. The crystal explorer 17.5 programme was utilised to visualise and investigate an intermolecular interactions and donor-acceptor interaction sites in this analysis. The red and blue patches shows how π … π stacking interaction in the molecule.

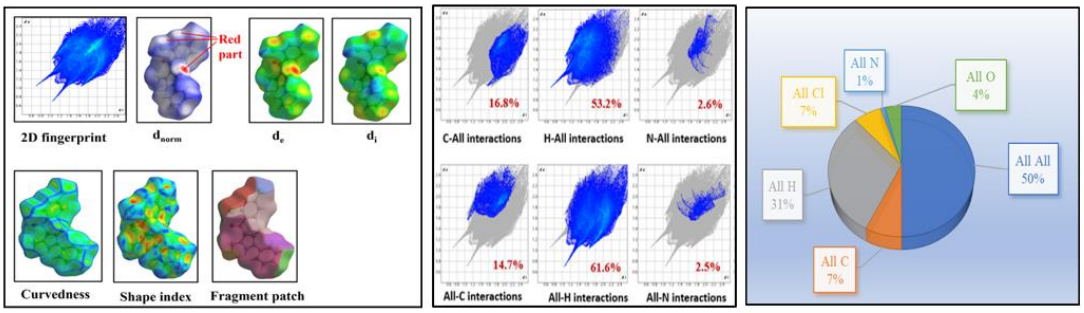

Fig.2.6. HOMO-LUMO molecular diagram of HL^{I} ligand

Conclusion

Three acylpyrazolone ligands were synthesized and characterized. Structural elucidation using FTIR spectral analysis shows significant vibrations. The single crystal data are largely used to examine their structure, geometry, composition, surface interactions, and lattice energy. The Hirshfeld surface analysis was also carried out to identify the crystal strength through interaction energies and intermolecular non-covalent surface interactions in the ligand.

Chapter 3: Synthesis, Characterization and Structural assessment of biologically active Square pyramidal Cu(II) acylpyrazolone complexes: DFT, Hirshfeld analysis

Part (a): Square pyramidal Cu(II) acylpyrazolone complex: Synthesis, characterization, crystal structure, DFT and Hirshfeld analysis, in-vitro anti-cancer evaluation

3a.1. Experimental work

3a.1.1. Synthetic route of complex-1

A hot methanolic solution of 1 eq Copper sulphate and 2 eq HL^{II} ligand were refluxed in a round bottom flask at 80-90°C. After refluxing the solution was filtered and the product was washed using hot methanol and dried. A few amounts of an obtained product was recrystalized in DMF solution.

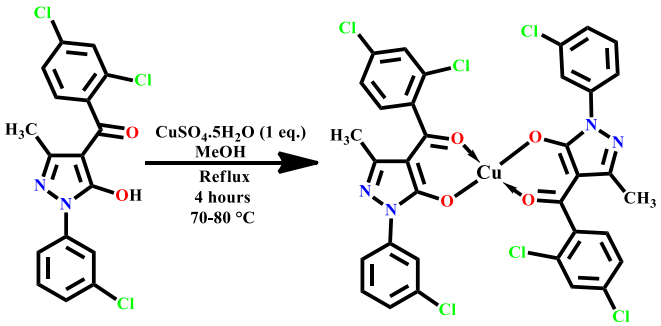

Fig.3.1. Synthetic route of complex-1

Complex-1; Colour: Green, **yield:** 83.00%, **M.P:** >200°C, **Molecular formula:** $C_{34}H_{20}CuCl_6N_4O_4$, **M.W:** 824.81, **Elemental analysis:** Exp.(C%=53.50,H%=2.91,N%=7.34), Calc. (C%=52.69,H%=2.80,N%=7.21).

3a.2. Results and discussion

3a.2.1. FTIR spectral studies

Table 3.1. FTIR spectral data of Ligands and Copper complex-1

Code	$\nu_{C=O}$ of benzoyl chloride	$\nu_{C=O}$ of pyrazolone	Cyclic$\nu_{(C=N)}$	C–H in plane deformation	ν_{M-O}
HL^{II}	1550	1524	1432	1216	-
Complex-1	1524	1591	1471	1162	628

3a.2.2 Thermogravimetric analysis

Three-step decomposition of 5 Co-ordinated complex-1 can be examined through the TGA analysis.. Degradation of both the ligands can be observe at the range of 280-500°C.

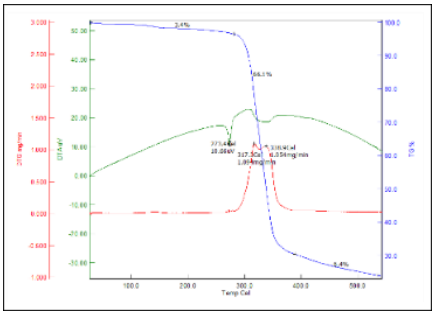

Fig.3.2. TG-DTA plot of complex-1

3a.2.3. Single crystal X-ray diffraction study

The geometry of a $[Cu(HL^{II})_2(DMF)]$ complex-1 was appear in the form of Square pyramidal (Penta coordinated) at which four Oxygen [O(1),O(2),O(3),O(4)] of ligand comprise the axial position and O(5) from DMF solvent molecule at equatorial position having Triclinic crystal system and P-1 space group.

$[Cu(HL^{II})_2(DMF)]$: Z= 2, α= 64.719°, β= 76.578(10)°, γ= 86.836(10)°, a= 10.994(2)Å, b= 14.227(3) Å, c= 15.761(3)Å

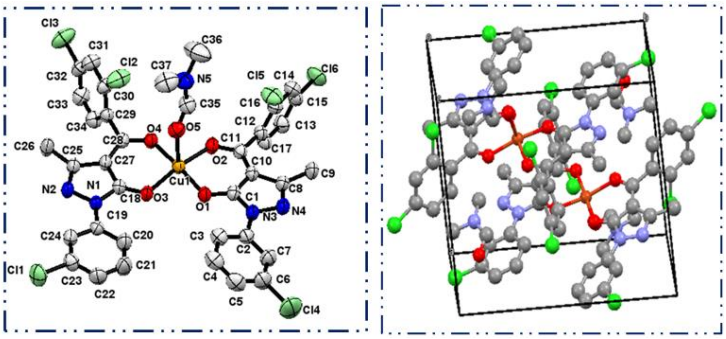

Fig.3.3. ORTEP view and crystal packing of $[Cu(L^{II})_2(DMF)]$ complex-1

3a.2.4. Computational analysis employing DFT

B3LYP/6-31G level basis set was used to compute the optimized geometry with energy value -182.454 keV for complex. Frontier orbitals have been studied because they are essential for determining chemical stability, energy value, and chemical behaviour. **Table 3.2. Global parameters of complex**

Properties	Mathematical Formula	$[Cu(L^{II})_2(DMF)]$
Ionization potential (IP)	$IP = -E_{HOMO}$	8.376
Chemical Potential (μ)	$\mu = 1/2 (E_{HOMO} + E_{LUMO})$	-5.21

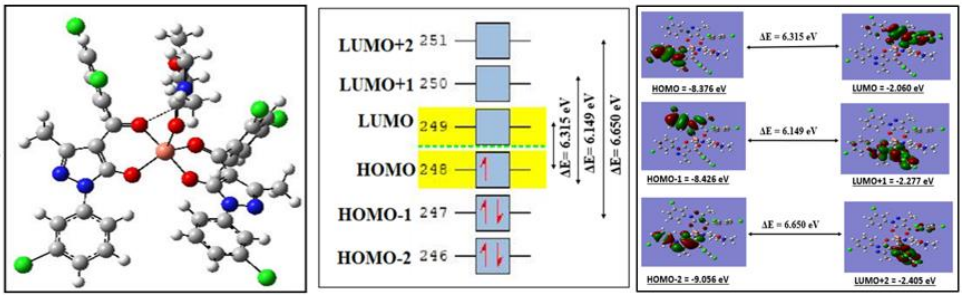

Fig.3.4. DFT optimized structure and HOMO-LUMO orbital of complex-1

3a.2.5. Spin density plot, MESP and NBO analysis

Spin densities may be calculated more informatively when an unpaired electron is present in the system. The coordinated donor atoms receive the negative spin densities, whereas the positive signed densities are scattered over the metal centre. MESP shows the molecular dimensions and electrostatic potential. The reddish region is most negative region and a bluish is moderate negative region, while green section indicates a potential midpoint among the two opposite ends. It is possible to measure the delocalization of electron density between occupied Lewis-type NBOs and unoccupied non Lewis type (acceptor/Reydberg) through NBO analysis which correlates to a stabilising donor-acceptor interaction. Cu has natural electronic configuration like: [core] 3d(9.11) 4s(0.29) 4p(0.38) accordingly.

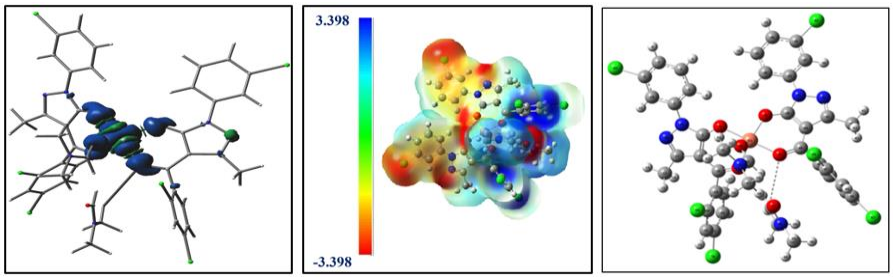

Fig.3.5. Spin density, MESP & NBO image of complex-1 respectively

3a.2.6. Hirshfeld surface analysis

This study has provided a thorough description of an immediate surroundings of the molecule. The crystal explorer 17.5 programme was utilised to visualise and investigate an intermolecular interactions and donor-acceptor interaction sites in this analysis. The red and blue patches shows how π … π stacking interaction in the molecule.

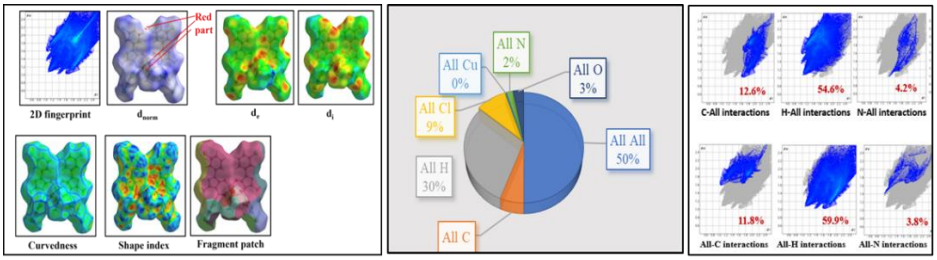

Fig.3.6. Molecular Hirshfeld & 2d finger print plot of complex-1

3a.2.7. Electronic spectral analysis

UV-visible absorption spectra of complex-1 were taken in DMSO solvent. A sharp absorption band at 277nm (36101cm^{-1}) is attributed to the LMCT (acylpyrazolone ligand) to the metal (Cu^{2+}). Furthermore, the complex exhibit *d-d* band at a shorter wavelength in the visible region at 800 nm (12500 cm^{-1}). A particular transition occurs from the $^{2}Eg \rightarrow {}^{2}T2g$ transition.

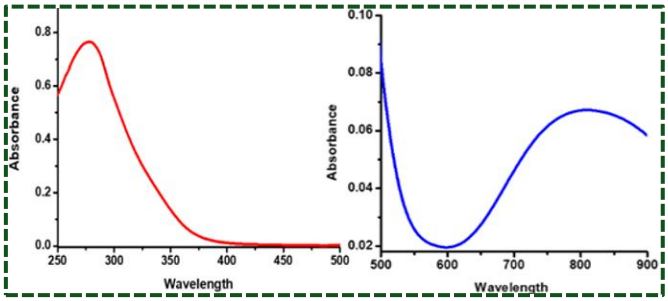

Fig.3.7. LMCT & d-d band of complex-1

3a.2.8. ESR analysis

The ESR spectral analysis was carried out through ESR JEOL analysis in Powder state at RT with tetracyanoethylene (TCNE) as a marker (g = 2.00277). Cu(II) exhibit four lines which can be seen from the graph. In this analysis $g_{\parallel (2.361)} > g_{\perp (2.050)} > 2.0023$ which suggesting the ground state results from $dx^2\text{-}y^2$ orbital.

3a.2.9. Electro-chemical analysis (CV)

The redox behaviour of copper complex was studied through cyclic voltammetry (CV) technique. Diagram shows the two oxidation and two reduction peaks. The value of ΔEp_1 is 0.5955 V and ΔEp_2 is 1.6433 V for each redox couple. Nature of the graph is quasi-reversible.

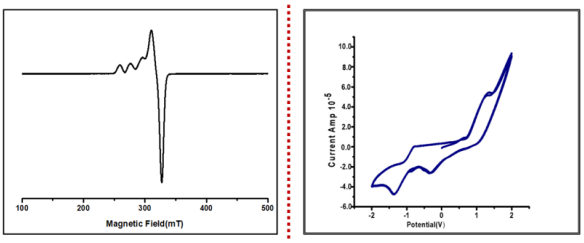

Fig.3.8. (A)X-band ESR spectra of complex-1 in the solid state at RT, (B) using 0.1 M TBAP at Scan rate (v) = 100 mV/s.

3a.2.10. Cytotoxicity assay

In vitro anticancer activity of complex-1 has been done against NCI-H23, SH-SY5Y and HepG2 cells. IC50 value of the copper complex was reported to be 5.4 µM, 7.2 µM, and 7.1 µM in NCI-H23, SH-SY5Y, and HepG2 cells respectively. Comparative study with cis platin is also reported.

3a.2.10.1. Cell death analysis & Scratch assay

Cell death analysis provides a count of both live and dead cells using calcein and EthD-1 dyes which is responsible for green fluorescence (indicates live cells) and red fluorescence (indicates dead cells) respectively. Remarkable cell death could be observed as shown by predominant red fluorescence. The scratch assay is a straightforward and economical method to study cell migration in vitro. It has been examined at three different times interval : at 0 h, 24 h and 48 h. At 24 h to determine the rate of cell migration. At 24hr near about 41% of the wound closer was seen in the control medium while 29% can be observed in treated condition.

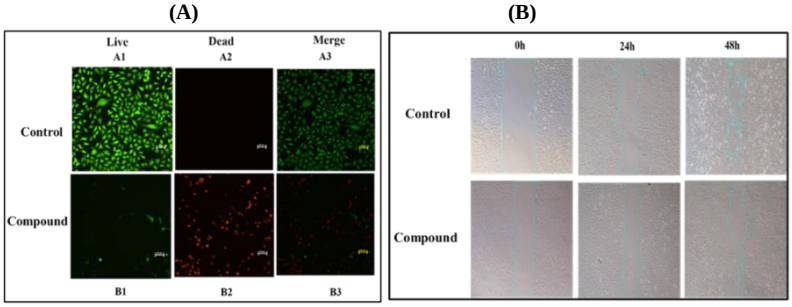

Fig.3.9. (A) Dual staining (live/dead assay) of NCI-H23 cells exposed to complex-1, (B) Scratch assay

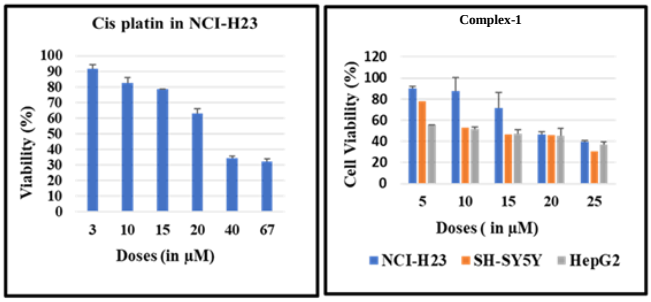

Fig.3.10. Percent viability of NCI-H23 Cells exposed to indicated doses of Cisplatin and complex-1

Conclusion

The present research demonstrates the pharmacological potency of pyrazolone derivatives and it's Copper(II) metal complex. Acylpyrazolone ligand and it's Copper(II) metal complex were synthesized and characterized using various spectroscopic methods. X-ray crystallography data suggested the square pyramidal geometry of complex and also gave an idea about the binding site of atoms in the complex. ESR study suggested the paramagnetic behaviour of a complex. Redox behaviour can be understood by CV. *In vitro* anticancer activity suggesting the encouraging application of complex.

Part (b): Acylpyrazolone based square pyramidal Cu(II) complexes: Synthesis, structural characterization, DFT and antiproliferative properties

3b.1. Experimental work

3b.1.1. Synthetic route of complex-2 & complex-3

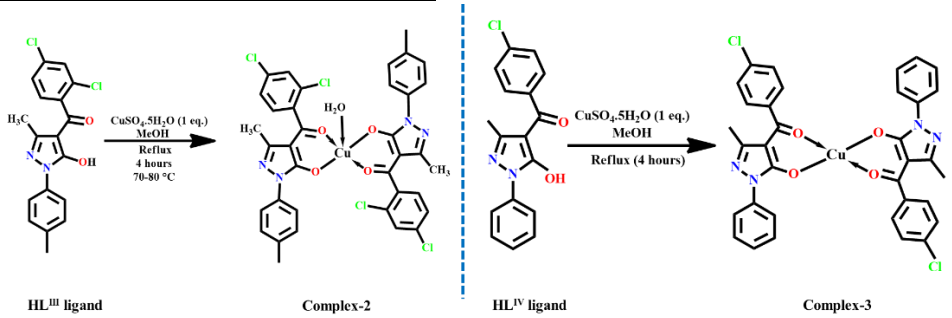

Fig.3.11. Synthetic route of complex-2 & complex-3

HL^{III} ligand (0.722g, 0.002 mol), **HL^{IV} ligand** (0.625g, 0.002 mol), **Copper sulphate** (0.249g of $CuSO_4.5H_2O$, 0.001mol) and CH_3OH (10mL).

Complex-2: **Colour**: Green, yield: 85.40%, M.P:> 200°C, Molecular formula: $C_{37}H_{30}CuCl_4N_4O_6$, **Crystal:** Pale green-yellow thick needle, **M.W:** 832.02, **Elemental analysis**: Anal. Calcd (%): C, 54.65; H, 3.88; N, 8.71; Found (%): C, 54.97; H, 3.98; N, 8.90, **FTIR(KBr, cm^{-1}):** 1598 ($\nu_{C=O}$ of pyrazolone), 1505 ($\nu_{C=O}$ of benzoyl), 1363 ($\nu_{C=N}$), **Molar conductance(10^{-3} DMF):** 3.27 $ohm^{-1}cm^2mol^{-1}$.

Complex-3: **Colour**: Green, yield: 84%, M.P: >200°C, Molecular formula: $C_{34}H_{24}CuCl_2N_4O_4$

Crystal: thick plates, M.W: 687.03, **Elemental analysis:** Anal. Calcd (%): C, 56.51; H, 3.95; N, 7.32; Found (%): C, 56.79; H, 4.10; N, 7.56, Metal estimation, gravimetrically and volumetrically, Cu = 8.04%. **FTIR(KBr, cm^{-1}):** 1597 ($\nu_{C=O}$ of pyrazolone), 1575 ($\nu_{C=O}$ of benzoyl), 1439 ($\nu_{C=N}$), **Molar conductance(10^{-3} DMF):** 3.86 $ohm^{-1}cm^2mol^{-1}$.

3b.2. Results and discussion

3b.2.1. FTIR spectral studies

Table 3.3. FTIR spectral data of ligands and copper complexes

Code	$\nu_{C=O}$ of benzoyl chloride	$\nu_{C=O}$ of pyrazolone	Cyclic$\nu_{(C=N)}$	C–H in plane deformation	ν_{M-O}
HL^{III}	1585	1668	1472	1213	-
Complex-2	1550	1598	1363	1161	603

3b.2.2. Thermogravimetric analysis

The aforementioned methodology can be used to evaluate three-step decomposition of complexes. Thermal breakdown of the copper at temperatures around 100 and 550 °C demonstrates the remarkable thermal stability of both complexes. CuO residue is stable till 550°C with a loss of 13.1%.

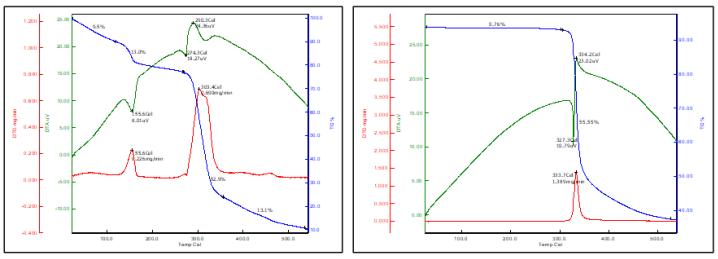

Fig.3.12. TG-DTA plot of complex-2 & complex-3 respectively

3b.2.3. Single crystal X-ray diffraction study

A geometry of the synthesized complexes appeared in the form of a Square pyramidal (Penta coordinated) by the single crystal analysis. Cu-O bond length in both the complexes is 180 A°. The bond distance between Cu-O(1) in **$[Cu(HL^{III})_2(DMF)]$** is 1.92(17) Å and **$[Cu(HL^{IV})_2(DMSO)]$** 1.92(9) Å respectively.

$[Cu(HL^{III})_2(DMF)]$: Z= 4, α= 90°, β= = 93.355(6)°, γ= 90°, a = 13.9750(19)Å, b= 6.8795(9) Å, c= 39.669(5)Å

$[Cu(HL^{IV})_2(DMSO)]$: Z= 2, α= 90°, β= 101.557(8)°, γ=90°, a = 14.415(4)Å, b= 16.478(4)Å, c= 14.620(4)Å

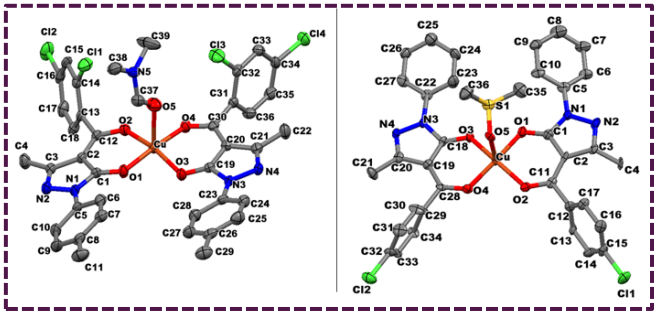

Fig.3.13. Thermal ellipsoid structure of complex-2 & complex-3 respectively

3b.2.4. Computational analysis employing DFT

The geometries were computed using B3LYP/LANL2DZ and B3LYP/6-31G levels for both complexes. The optimization energy of $[Cu(HL^{III})_2(DMF)]$ and $[Cu(HL^{IV})_2(DMSO)]$ complexes is -65.6225 keV and -60.4222 keV respectively when computed at B3LYP/LANL2DZ. The observed energy is -139.7153 keV and -134.5150

keV while utilizing B3LYP/6-31G basis set. For a variety of chemical interactions, the HOMO-LUMO energies are essential. **Table 3.4. Global parameters of two copper complexes**

Properties	Mathematical Formula	Complex-2	Complex-3
Ionization potential (IP)	$IP = -E_{HOMO}$	5.794	5.95
Chemical Potential (μ)	$\mu = 1/2 (E_{HOMO} + E_{LUMO})$	-3.82	-4.02

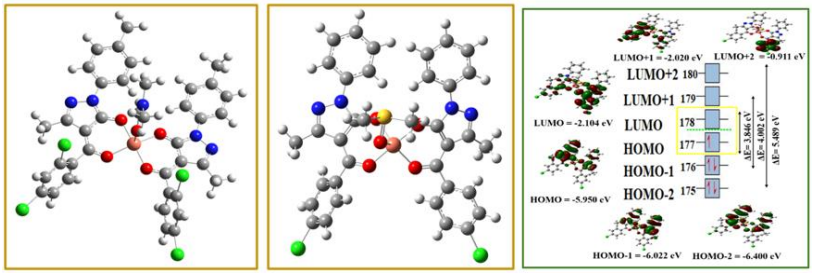

Fig.3.14. Thermal ellipsoid structure of complex-2 & complex-3

3b.2.5. Hirshfeld surface analysis

Which gives an idea about the interaction and hydrogen bonding. By defining different colours for short and long contacts, the HS displayed over dnorm enables the investigation of H-bonding interactions. The de and di stand for the separation between the Hirshfeld surface and the closest external/internal atom.

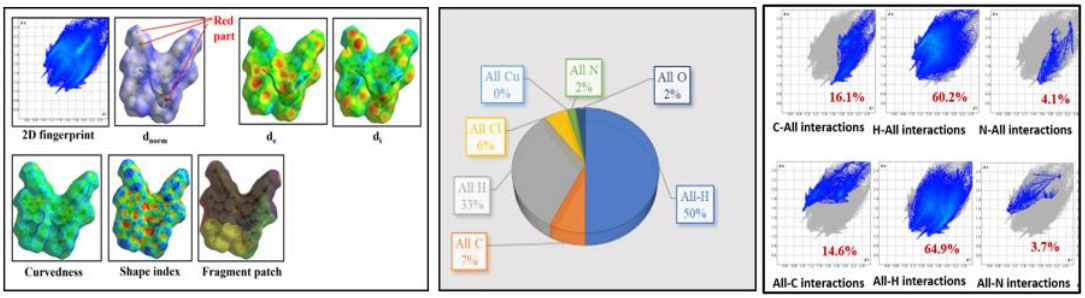

Fig.3.15. Molecular hirshfeld diagram and 2d fingerprint plot of complex-2

3b.2.6. Electronic spectral analysis

The crystal sample underwent UV-visible absorption investigations up to 950 nm to determine the energy gap of copper complexes. DMSO solvent was used for the analysis. The absorbance of a transition can be categorised as the $d_{x^2-y^2} \rightarrow d_{xz}$, d_{yz}, and $d_{x^2-y^2} \rightarrow d_{z^2}$ it is because of the Jahn-Teller distortion in the complexes. The specific transition follows the $^2E_g \rightarrow {}^2T_{2g}$ transition. The specific transition follows the $^2E_g \rightarrow {}^2T_{2g}$ transition. Which interpreted as a Square Pyramidal geometry of both complexes.

Complex-2: d-d transition (768 nm), Molar absorbance (ε): 89.1 M^{-1} cm^{-1}

Complex-3: d-d transition (751 nm) Molar absorbance (ε): 57.1 M^{-1} cm^{-1}

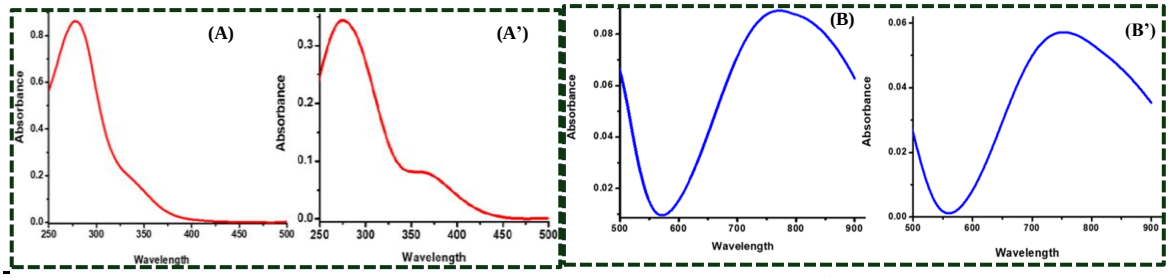

Fig.3.16. (A)&(A') LMCT spectra of complex-2 & complex-3, (B)&(B') d-d spectra of complex-2 & complex-3 respectively

3b.2.7. ESR analysis

To explain the magnetic behaviour of the copper complexes ESR analysis was done Tetracyanoethylene (TCNE) was used as a marker (g = 2.00277) during the ESR JEOL analysis in the Powder state at RT at in the solution state at LNT. The graph shows four lines that represent Cu(II). The value of $g_{\|}$ at RT is 2.545 and at LNT is found to be 2.353 for complex-2 while for the complex-3.

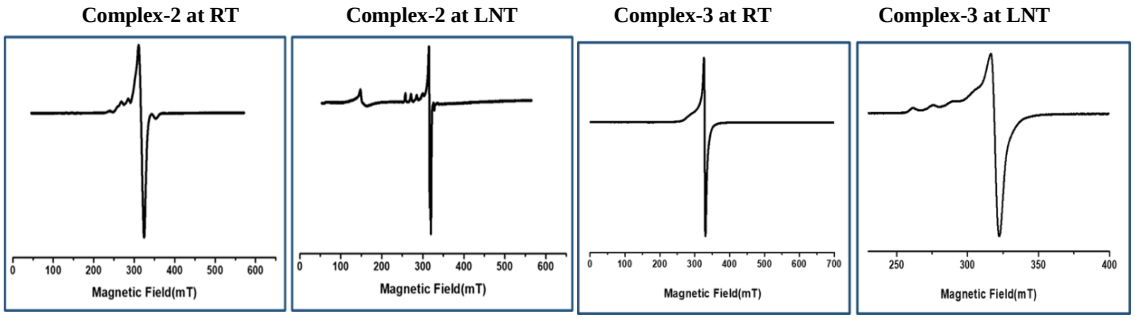

Fig.3.17. X-band ESR spectra of complex-2 & complex-3 in the solid state at RT and LNT

3b.2.8. Cytotoxicity assay

In vitro anticancer activity of a complex-2 has been done against NCI-H23, SH-SY5Y and HepG2 cells. IC50 value is 4.8 µM, 11.41 µM, and 11.07 µM respectively. While complex-3 assessed against SH-SY5Y cancer cells since this complex shows greater effectivity against the SH-SY5Y cell line hence we are reporting IC_{50} value of this complex on neuroblastoma cancer cells which is 10.8 µM. Comparative study with cis platin is also reported.

3b.2.8.1. Cell death analysis & Scratch assay

Cell death analysis provides a count of both live and dead cells using calcein and EthD-1 dyes which is responsible for green fluorescence (indicates live cells) and red fluorescence (indicates dead cells) respectively. The scratch assay is a straightforward and economical method to study cell migration in vitro. It has been examined at three different times interval : at 0 h, 24 h and 48 h. At 24 h to determine the rate of cell migration.

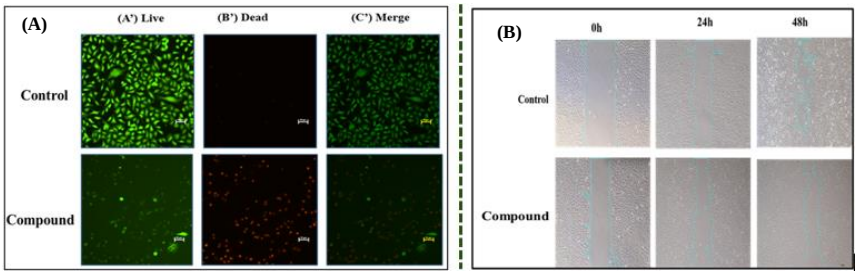

Fig.3.18. (A) Dual staining (live/dead assay) of NCI-H23 cells exposed to complex-2, (B) Scratch assay

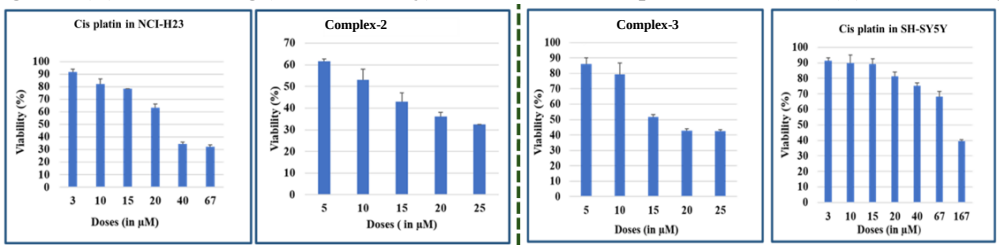

Fig.3.19. (i)Percent viability of NCI-H23 Cells exposed to indicated doses of Cisplatin & complex-2
(ii) Percent viability of NCI-H23 Cells exposed to indicated doses of Cisplatin and complex-3

Conclusion

The design and synthesis of pyrazoles is a promising topic of research since they are an important pharmacophore with a diversity of biological characteristics. In this research we discussed the synthesis and characterization of the ligand and complex-2 & complex-3. Square Pyramidal geometry of the stable copper complexes demonstrated by single crystal X-ray crystallography. B3LYP/6-31G and B3LYP/LANL2DZ two different basis set were used to optimized both complexes. *In vitro* anticancer activity indicates the positive application of the complex. We found that lung cancer cells' ability to survive and spread can be inhibited by the complex-2.

Chapter 4: Synthesis of New Square planar Cu(II) complexes derived from acylpyrazolone ligand: Molecular structure Computational, Hirshfeld analysis and antiproliferative properties

Part (a): Cytotoxicity assay and gene expression studies of acylpyrazolone-based square planar Cu(II) complexes: synthesis, characterization and computations

4a.1. Experimental work

4a.1.1. Synthetic route of complex-4 & complex-5

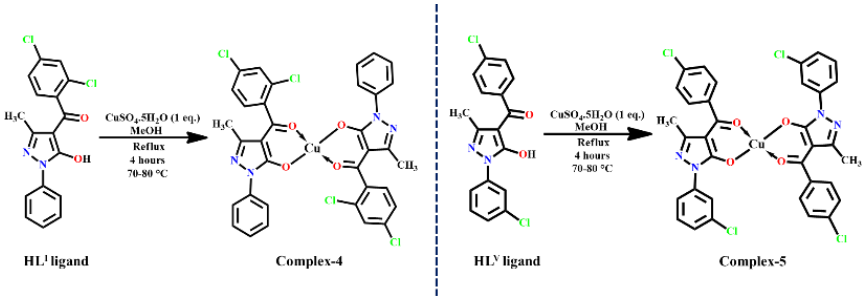

Fig.4.1. Synthetic route of complex-4 & complex-5

HL^{VII} ligand (0.694g, 0.002 mol), **HL^{V} ligand** (0.694g, 0.002 mol), **$CuSO_4.5H_2O$** (0.249g, 0.001mol) and CH_3OH (10mL).

Complex-4: **Colour**: Green, yield: 85%, M.P:> 200°C, Molecular formula: $C_{34}H_{22}CuCl_4N_4O_4$, **Crystal:** Dark green crystal, M.W: 755.92, **Elemental analysis**: C (Exp. 53.92%, Calc. 54.02%); H (Exp. 2.90%, Calc. 2.93%); N (Exp. 6.96%, Calc. 7.41%); Cu = 8.03 %, **FTIR(KBr, cm^{-1}):** 1602 ($\nu_{C=O}$ of pyrazolone), 1577 ($\nu_{C=O}$ of benzoyl), 1435 ($\nu_{C=N}$), 508($\nu_{Cu=O}$), **Molar conductance(10^{-3} DMF):** 3.27 $ohm^{-1}cm^2mol^{-1}$.

Complex-5: **Colour**: Green, yield: 86 %, M.P: >200°C, Molecular formula: $C_{34}H_{22}CuCl_4N_4O$, **Crystal:** Dark green crystal, M.W: 755.92, **Elemental analysis**: C (Exp. 49.20%, Calc.: 49.49%); H (Exp. 3.03%, Calc. 3.03%); N (Exp. 7.50%, Calc. 7.80%); Cu = 8.00%, **FTIR(KBr, cm^{-1}):** 1601 ($\nu_{C=O}$ of pyrazolone), 1586 ($\nu_{C=O}$ of benzoyl), 1475($\nu_{C=N}$), 490($\nu_{Cu=O}$), **Molar conductance(10^{-3} DMF):** 2.18 $ohm^{-1}cm^2mol^{-1}$.

4.2. Results and discussion

4a.2.1. FTIR spectral studies

Table 4.1. FTIR spectral data of ligands and copper complex

Code	$\nu_{C=O}$ of benzoyl chloride	$\nu_{C=O}$ of pyrazolone	Cyclic$\nu_{(C=N)}$	C–H in plane deformation	ν_{M-O}
HL^I ligand	1587	1627	1515	1394	-
Complex-4	1577	1602	1435	1379	508

4a.2.2. Thermogravimetric analysis

The copper complex thermally decomposes between 100 and 550°C, demonstrating the remarkable thermal stability of complex. Degradation of ligand moiety is 76.5% and 63.5% in complex-4 and complex-5 respectively.

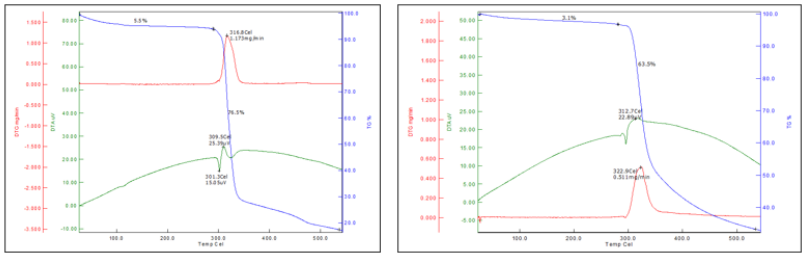

Fig.4.2. TG-DTA graph of complex-4 & complex-5 respectively

4a.2.3. Single crystal X-ray diffraction study

Molecular crystal structure of copper complexes is green in colour were obtained after the complexation reaction with acypyrazolone ligand and recrystallized in DMF solvent. The geometry of synthesized complexes appeared in the form of Square Planar. Crystal of complex-4 has triclinic and complex-5 has monoclinic crystal system.

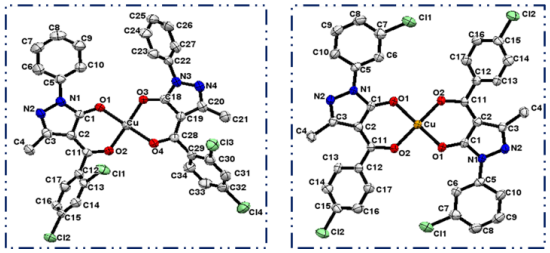

Fig.4.3. Thermal ellipsoid plot (with 55% probability) of complex-4 & complex-5 respectively

$[Cu(HL^{I})_2]$ complex-4: α= 90.834(4)°, β= 95.017(4)°, γ=106.124(4)°, a = 9.6075(12)Å, b= 11.7452(15)Å, c= 14.3696(17)Å

$[Cu(HL^{V})_2]$ complex-5: = 90°, β= 111.660(4)°,γ=90°, a = 9.0930(11)Å, b= 27.412(3)Å, c= 6.8238(8)Å

4a.2.3.1. Powder XRD analysis

A simulated pattern for both complexes was derived from the single crystal data and compared to the experimental pattern from the powder XRD experiment. A sharp band with maxima 2θ = 20 to 25° range for complex-4 while 2θ = 5 to 10° range for complex-5 has been seen in the XRD graph. This ascertain that bulk products are essentially the same as those exist in single crystal form.

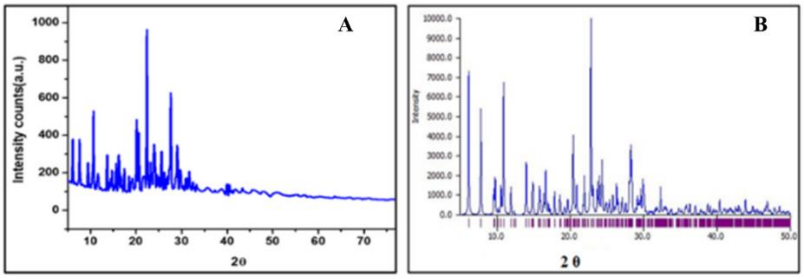

Fig.4.4. (A) Experimental powder XRD pattern & (B) Simulated powder XRD pattern of complex-4

4a.2.4. DFT based Computational analysis

The geometry optimization of complex-4 and complex-5 were done via B3LYP/6-31G level basis set using Gauss View 6.0 software. The energy value for complex-4 and complex-5 are -49.934 keV, -144.475 keV, -144.475 keV. HOMO-LUMO energies play an essential role to determine a variety of chemical interaction.

Table 4.2. Global parameters of complexes

Properties	Mathematical Formula	Complex-4	Complex-5
Ionization potential (IP)	$IP = -E_{HOMO}$	5.79	6.05
Chemical Potential (μ)	$\mu = 1/2 (E_{HOMO} + E_{LUMO})$	-3.82	-4.10

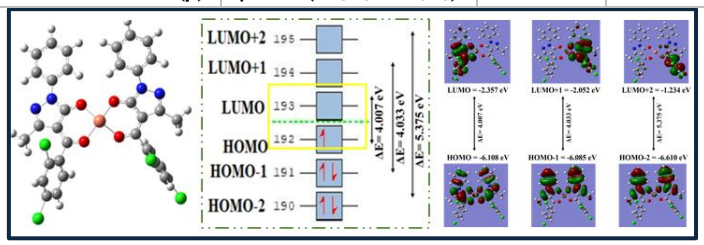

Fig.4.5. DFT optimized geometry & HOMO-LUMO orbital of complex-4

4a.2.4.1. Spin density plot

Electronic spin density is positive and scattered over the metal centre while in regions where electrons are more likely to be found in the β spin state, it is negative.

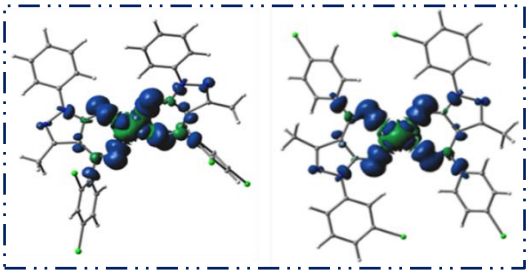

Fig.4.6. Spin density plot of complex-4 & complex-5

4a.2.4.2. Molecular electrostatic potential (MESP) & Natural bond orbital (NBO) analysis

The electron density particularly corresponds to the MESP is a highly significant aspect when studying the interactions across hydrogen bonds, Electrophilic and Nucleophilic sites as well as their ability to react. The region with the largest negative, positive and zero ESP values is represented by the coloured shades red, blue, and green, respectively. Through NBO analysis, it is possible to measure the delocalization of electron density between

occupied Lewis-type NBOs (donor) and unoccupied non-Lewis-type NBOs. In complex-4 and complex-5 the natural atomic charges on Cu^{+2} are +1.1676 and +1.1731 respectively

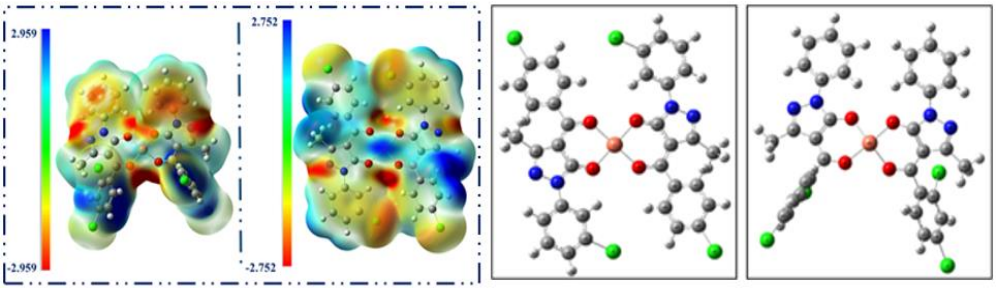

Fig.4.7. MESP & NBO image of complex-4 & complex-5

4a.2.5. Hirshfeld surface area analysis

With the help of Crystal Explorer 17.5 program, the donor-acceptor interaction sites and intermolecular contacts can be visualized in this analysis 3D Hirshfeld surfaces have been mapped over dnorm, de, di, shape index, curvedness and fragment patch.

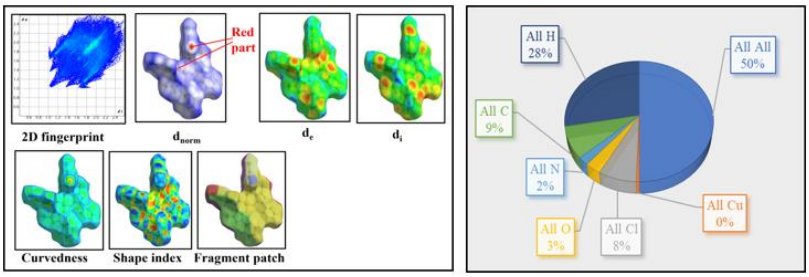

Fig.4.8. Molecular hirshfeld diagram of complex-5

4a.2.6. Electronic spectral analysis

The UV-visible absorption spectroscopy has been extensively used for providing the structural information of a compound. The electronic spectra of Square Planar complex-4 and complex-5 were recorded in a DMSO. The crystal sample underwent UV-visible absorption investigations up to 950 nm to determine the energy gap of copper complexes. DMSO solvent was used for the analysis. The particular transition occurs from the $^2E_g \rightarrow {}^2T_{2g}$ transition.

Complex-4: π-π*(277 nm), n-π*(333 nm), d-d transition (742 nm)

Complex-5: π-π*(283 nm), n-π*(352 nm), d-d transition (739 nm)

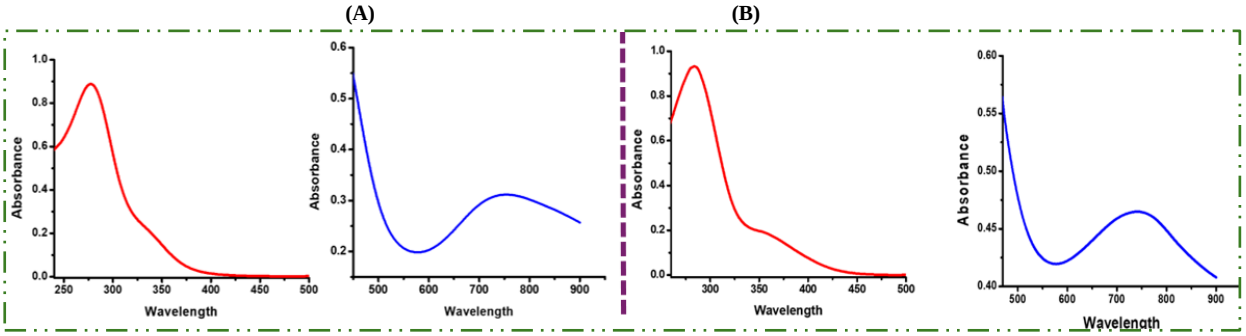

Fig.4.9. (A) LMCT & d-d band of complex-4 respectively, (B) LMCT & d-d band of complex-5 respectively

4a.2.7. ESR analysis (magnetic behaviour)

The ESR spectral analysis of two copper complexes were carried out through ESR JEOL analysis in Powder state at RT and in solution state at LNT with tetracyanoethylene (TCNE) as a marker (g = 2.00277) to explain the geometry of copper complex. **Table 4.3. Parameters from ESR spectra of complex-4 &5**

LNT	Complex-4	Complex-5
$g_{\|}$	2.370	2.313
$g_{\perp}$	2.063	2.052
$A_{\|}$ (10^{-4} cm^{-1})	166	151
$A_{\perp}$ (10^{-4} cm^{-1})	29	76

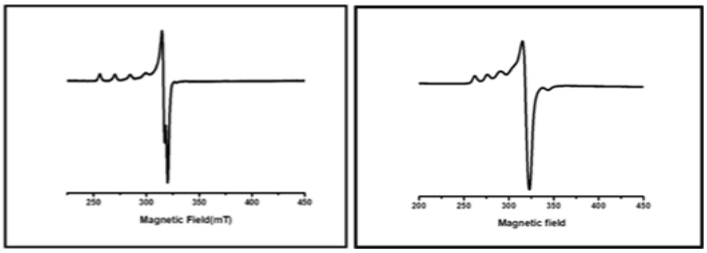

Fig.4.10. X-band ESR spectra of complex-4 & complex-5 in the solution state at LNT respectively

4a.2.8. Electro-chemical analysis (CV)

The redox behaviour of complex-4 & complex-5 were studied through cyclic voltammetry (CV) technique. An anodic oxidation peak Epa(I) = -0.6441V (Cu^{0+}→Cu^{+1}) and Epa(II) = 1.3991V (Cu^{1+}→Cu^{+2}) observed and reduction peak Epc(I) = -1.0977V (Cu^{2+}→Cu^{+1}) and Epc(II) = -0.3303V (Cu^{1+}→Cu^{+0}) observed for complex-4.

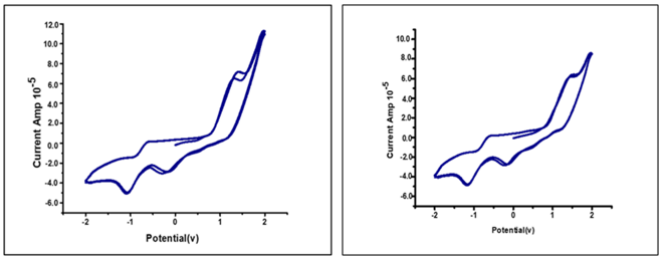

Fig.4.11. Cyclic voltammogram of complex-4 &5 in DMSO solution using 0.1 M TBAP at Scan rate 100

4a.2.9. Cytotoxicity assay

Cell viability was assessed using an MTT assay. The copper complexes were able to inhibit the cell viability of NCI-H23, SH-SY5Y and HepG2 cancer cells. IC50 was calculated against Cisplatin on SH-SY5Y neuroblastoma cancer cell line. The IC50 value is 44.94µM for cisplatin. Complex-5 gave the best result against SH-SY5Y cell line. Hence further study has been done on a complex-5. Such as Live/dead assay and Gene expression study by qRT-PCR against BAD and BCL2L1 genes. IC_{50} value for complex-4 is 7.2 µM, 12.3 µM, and 9.0 µM and complex-5 was reported to 8.4 µM, 8.4 µM, and 10.7 µM against NCI-H23, SH-SY5Y, and HepG2 cells respectively.

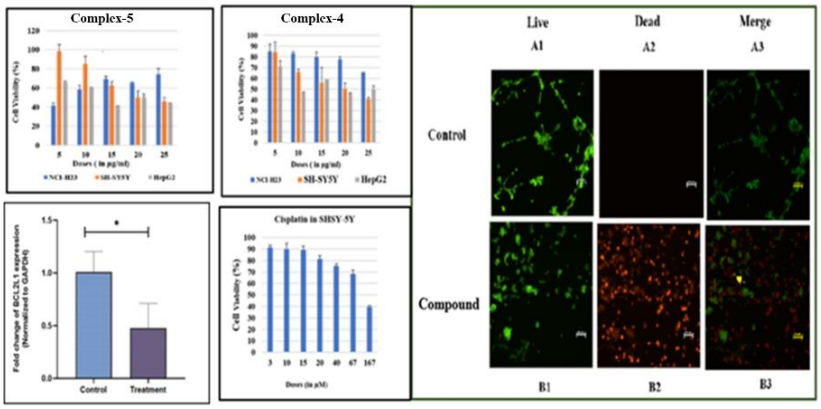

Fig.4.12. Percent viability of NCI-H23, SH-SY5Y and HepG2 Cells exposed to indicated doses of complex-4&5, NCI-H23 cells exposed to indicated dose of cisplatin, Live/dead assay of SH-SY5Y cells exposed to complex-5

Conclusions

The formation of two copper (II) complexes based on acyl pyrazolone ligand has been done and characterized. Keto form of synthesized ligand and the geometry around copper center is Square Planar proved by X-ray crystallography technique. Ligand and complexes were optimized via DFT/B3LYP/6-31G method. ESR study suggested the paramagnetic behaviour of complex. To study the intermolecular interactions Hirshfeld surface analysis was employed. *In vitro* anticancer activity suggesting the encouraging application of both the complexes.

Part (b): Two New Square Planar Cu(II) complexes derived from a heterocyclic Pyrazolone ligand: Synthesis, In vitro anticancer activity, DFT and Hirshfeld analysis

4b.1. Experimental work

4b.1.1. Synthetic route of complex-6, complex-7

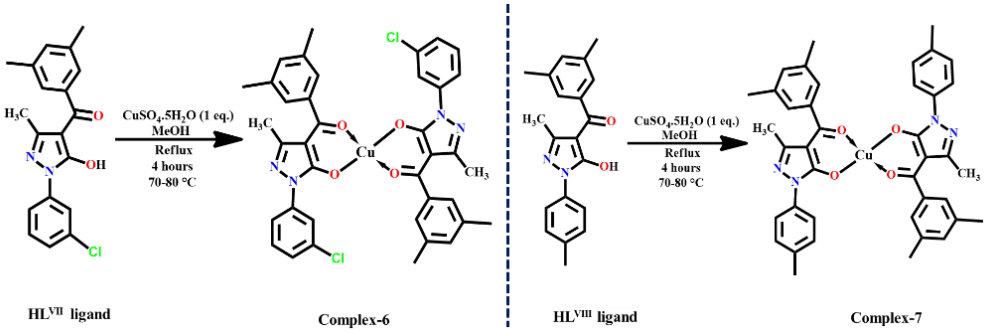

Fig.4.13. Synthetic route of complex-6 &7

HL^{VII} ligand (0.681g, 0.002 mol), **HL^{VIII} ligand** (0.640g, 0.002 mol), **Copper sulphate** (0.249g of $CuSO_4.5H_2O$, 0.001mol) and CH_3OH (10mL).

Complex-6: **Colour**: Green, yield: 82%, M.P:> 200°C, Molecular formula: $C_{38}H_{32}CuCl_2N_4O_4$, **Crystal:** Pale green-yellow thick needle, M.W: 743.14, **Elemental analysis**: C (Exp. 60.97%, Calc.: 61.42%); H (Exp. 4.86%, Calc. 4.34%); N (Exp. 7.44%, Calc. 7.54%); Cu = 8.03 %, **FTIR(KBr, cm^{-1}):** 1585 ($\nu_{C=O}$ of pyrazolone), 1603 ($\nu_{C=O}$ of 3,5-dimethyl benzoyl), 1485 ($\nu_{C=N}$), 596 ($\nu_{Cu=O}$), **Molar conductance(10^{-3} DMF):** 4.0 $ohm^{-1}cm^2mol^{-1}$,

Complex-7: **Colour**: Green, yield: 80 %, M.P: >200°C, Molecular formula: $C_{40}H_{38}CuN_4O_4$, **Crystal:** thick plates, M.W: 702.30, **Elemental analysis** C (Exp. 67.95%, Calc.: 68.41%); H (Exp. 5.30%, Calc. 5.45%); N (Exp. 7.15%, Calc. 7.98%); Cu = 8.00%, 1526 ($\nu_{C=O}$ of pyrazolone), 1593 ($\nu_{C=O}$ of benzoyl), 1492 ($\nu_{C=N}$), 513 ($\nu_{Cu=O}$), **Molar conductance(10^{-3} DMF):** 4.5 $ohm^{-1}cm^2mol^{-1}$.

4b.2. Results and discussion

4b.2.1. FTIR spectral studies

Table 4.4. FTIR spectral data of ligands and copper complexes

Code	$\nu_{C=O}$ of benzoyl chloride	$\nu_{C=O}$ of pyrazolone	Cyclic$\nu_{(C=N)}$	C–H in plane deformation	ν_{M-O}
HL^{VII}	1589	1621	1521	1377	-
Complex-6	1585	1603	1521	1379	596

4b.2.2. Thermogravimetric analysis

The mass loss and thermal stability of the material are inferred via thermogravimetric analysis (TGA). Thermal breakdown of the copper at temperatures around 100 and 550 °C demonstrates the remarkable thermal stability of both complexes. TGA analysis of the complex-6 & complex-7 revealed a total weight loss of 61.8% ,49.64% on TG graph respectively.

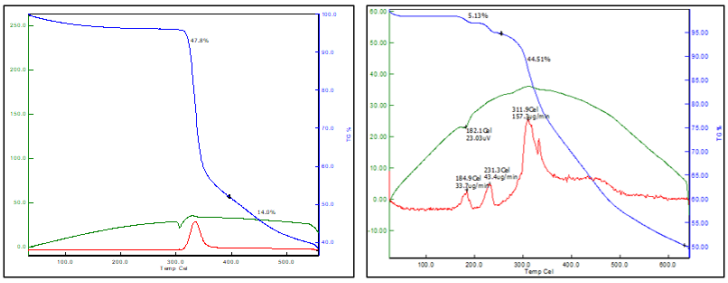

Fig.4.14. TG-DTA graph of complex-6 & complex-7 respectively

4b.2.3. Single crystal X-ray diffraction study

A geometry of the synthesized complexes appeared in the form of a Square Planner (Tetra coordinated) by the single crystal analysis. Cu-O bond length in both the complexes is 180 A°. The bond distance between Cu-O(1) in complex-6 & complex-7 is 1.917(12) Å and 1.910(19) Å respectively.

$[Cu(HL^{VII})_2]$: Z= 2, α= 90°, β= 97.8400(10)°, γ= 90°, a = 8.4243(2)Å, b= 27.7723(4)Å, c= 7.01630(10)Å

$[Cu(HL^{VIII})_2]$: Z= 2, α= 90°, β= 98.035(4)°, γ=90°, a = 7.2657(3)Å, b= 13.4359(4)Å, c= 18.2180(8)Å

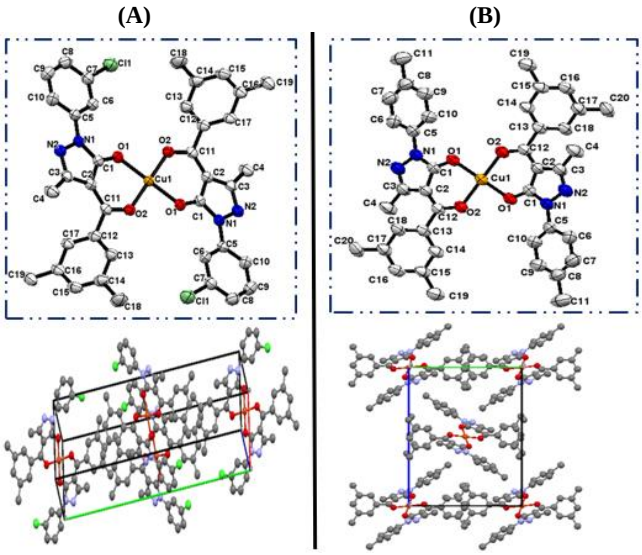

Fig.4.15. Thermal ellipsoid plots with a 55% probability, Packing configuration along a-axis of (A) complex-6 (B) complex-7

4b.2.4. Computational analysis employing DFT

The geometries were computed using B3LYP/LANL2DZ levels for both complexes. The optimization energy -123.7430 keV and -100.8708 keV respectively were observed for complex-6 & complex-7. Such negative energy value describe that both the complexes have covalent character. For a variety of chemical interactions, the HOMO-LUMO energies are essential. **Table 4.5. Global parameters of complexes**

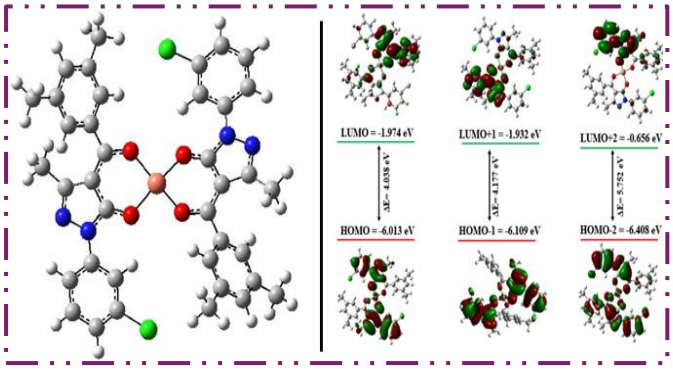

Fig.4.16. DFT optimized geometry & HOMO-LUMO diagram of complex-6

Properties	Mathematical Formula	Complex-6	Complex-7
Ionization potential (IP)	IP = - E_{HOMO}	6.01	5.60
Chemical Potential (μ)	μ = 1/2 (E_{HOMO} + E_{LUMO})	-3.99	-3.70
Softness (S)	S = 1/2η	0.24	0.26

4b.2.4.1. Spin density plot & NBO analysis

Natural Bond Orbital (NBO) analysis is a useful technique for the chemical interpretation of hyperconjugative interaction and electron density transfer from the filled lone pair electron. Cu^{+2} has 1.1676 natural atomic charges in complex-7 and 1.1638 in complex-6. The natural electrical arrangement of a copper in both the complexes is [core] 3d (9.13) 4s (0.34) 4p (0.36). Spin densities may be calculated more informatively when an unpaired electron is present in the system. electronic spin density is positive and scattered over the metal centre while in regions where electrons are more likely to be found in the β spin state, it is negative.

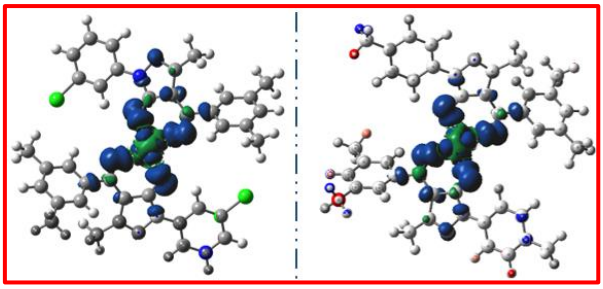

Fig.4.17. Spin density plot of complex-6 & complex-7 respectively

4b.2.5. Hirshfeld surface analysis

The closed intermolecular atomic contacts in the crystal structure were measured and visualised using Hirshfeld surface analysis. Hirshfeld surface (HS), this illustrates the hydrogen bonding and interaction. The short and extended interactions are shown, respectively, by red and blue areas.

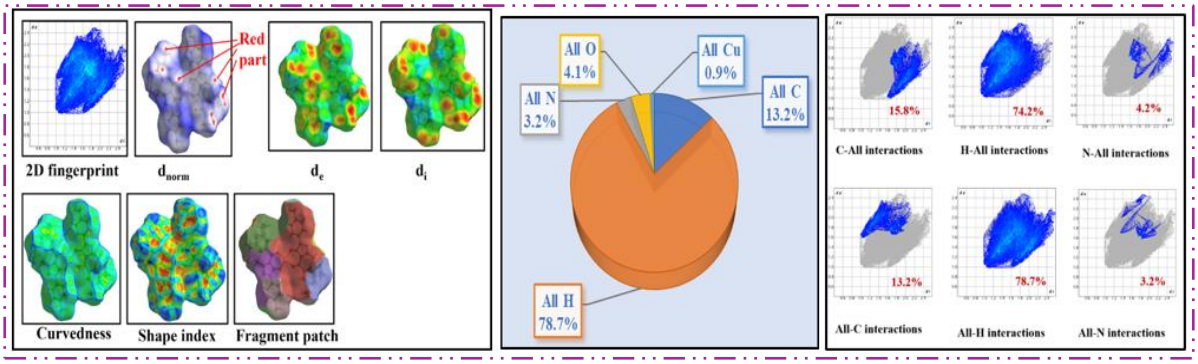

Fig.4.18. Molecular hirshfeld diagram & 2d fingerprint plot of complex-7

4b.2.6. Electronic spectral analysis

The crystal sample underwent UV-visible absorption investigations up to 950 nm to determine the energy gap of copper complexes. DMSO solvent was used for the analysis.

Complex-6: π-π*(282 nm), n-π*(358 nm), d-d transition (705 nm), Molar absorbance (ε): 36.9 M^{-1} cm^{-1}

Complex-7: π-π*(278 nm), n-π*(375 nm), d-d transition (706 nm) Molar absorbance (ε): 36.9 M^{-1} cm^{-1}

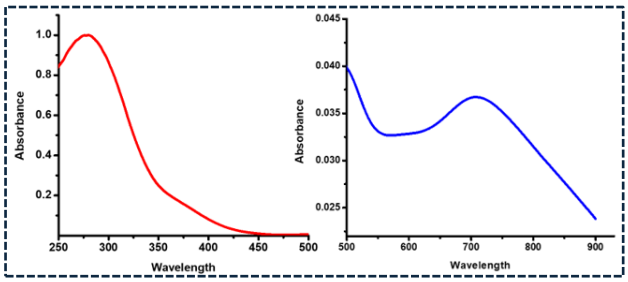

Fig.4.19. LMCT & d-d band of complex-7

4b.2.7. ESR analysis

ESR analysis was carried out at 77K (LNT) in solution state using an X band to clarify the magnetic behaviour of the copper complexes. Tetracyanoethylene (TCNE) was used as a marker (g = 2.00277). The value of $g_{\|}$ at LNT is found to be 2.3562, and $g_{\perp}$ is 2.0690. The value of g tensor is $g_{\|} > g_{\perp} > 2.0023$ supports the Square Planner geometry. A geometric parameter G value is found to be 5.1623 by this formula $G = (g_{\|} - 2.0023)/(g_{\perp} - 2.0023)$.

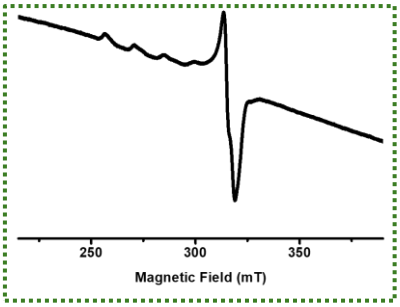

Fig.4.20. X-band ESR spectra of in the solution state at LNT

4b.2.8. Cytotoxicity assay

Cell viability was assessed by MTT assay. Three different cancer cell lines- NCI-H23(lung cancer), HepG2(Liver cancer), SH-SY5Y(neuroblastoma) were used against complex-7 to check an antiproliferative activity. As per the analysis complex-7 gave the best result on SH-SY5Y(Neuroblastoma cancer cells) because of its lower IC50 value (3.9 µM). IC50 value of cis platin was recorded 44.9 µM, this surpasses the complex's IC50 value. The outcomes indicate that the synthesized copper complex is more effective than cisplatin

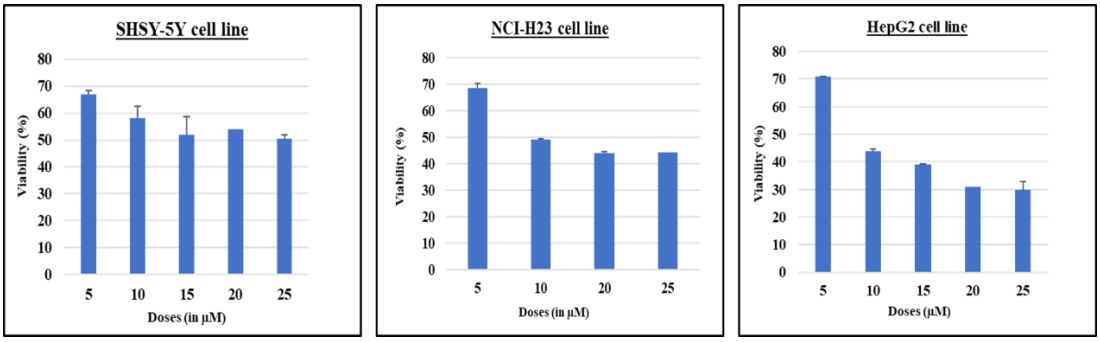

Fig.4.21. Percent viability of NCI-H23, SH-SY5Y and HepG2 Cells exposed to indicated doses of complex-7

Conclusion

We successfully investigated new Copper(II) complexes with Square Planar geometry. A variety of analytical techniques were employed for the characterization. Computational study of the synthesized compounds was studied using B3LYP/LanL2DZ basis set and the HOMO-LUMO energy gap was calculated. X band ESR measurement at LNT was used to establish the complexes' magnetic properties. Lower IC_{50} value inspired the complex to compare with the well-known drug Cis platin against SH-SY5Y cancer cells.

Chapter 5: Synthesis, Structural assessment of a series of three Octahedral Ni(II) Complexes with heterocyclic Acylpyarazolone ligand: Crystal structure, DFT-NBO analysis, Hirshfeld and Magnetic study

5.1. Experimental work

5.1.1. Synthetic route of complex

Hot ethanolic solution of HL^{VIII} ligand, HL^{IV} ligand and HL^{VI} ligand and Nickel metal salt were taken in three different round-bottom flasks attached to water condenser. The resulting mixture was refluxed for eight to ten hours at 70-80°C temperature in three separate round-bottom flasks. After Reflux, Pale green precipitates of all three synthesized Nickel complexes were produced. HL^{VIII}, HL^{IV}, HL^{VI} all three ligands have already been reported in the previously published articles by our lab [5][7].

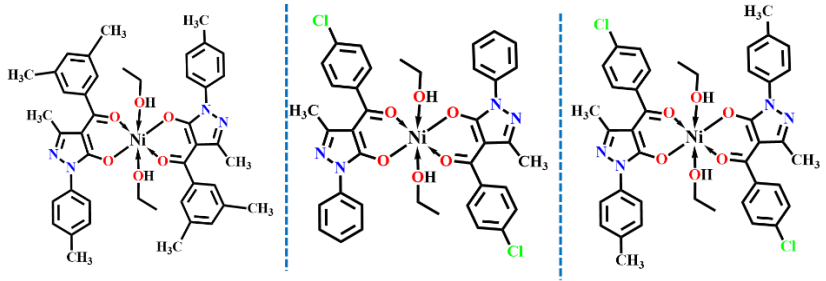

Complex-8 Complex-9 Complex-10

HL^{VIII} ligand (0.6403g, 0.002 mol), **HL^{IV} ligand** (0.625g, 0.002 mol), **HL^{VI} ligand** (0.653g, 0.002 mol), **Ni metal salt** (0.262g, 0.001 mol)

Complex-8: Pale bluish green crystal, yield: 81%, M.P:> 200°C, Molecular formula: $C_{44}H_{50}N_4NiO_6$, **M.W**: 789.58, Metal estimation, gravimetrically and volumetrically, **Elemental analysis**: C (Exp. 65.39%, Calc.: 66.19%); H (Exp. 6.3%, Calc. 6.3%); N (Exp. 7.30%, Calc. 7.54%); Ni = 8.4%, **Molar conductance:** 3.10 $ohm^{-1}cm^2mol^{-1}$, **FTIR(KBr, cm^{-1}):** 1602 ($\nu_{C=O}$ of pyrazolone), 1540 ($\nu_{C=O}$ of benzoyl), 1486 ($\nu_{C=N}$).

Complex-9: Pale bluish green crystal, yield: 81%, M.P:> 200°C, Molecular formula: $C_{38}H_{36}Cl_2NiN_4O_6$, **M.W**: 774.32, Metal estimation, gravimetrically and volumetrically, **Elemental analysis**: C (Exp. 57.39%, Calc. 58.10%); H (Exp. 4.20%, Calc. 4.60%); N (Exp. 8.23%, Calc. 8.88%); Ni = 8.4%, **Molar conductance:** 2.18 $ohm^{-1}cm^2mol^{-1}$, **Molar conductance:** 2.18 $ohm^{-1}cm^2mol^{-1}$, **FTIR(KBr, cm^{-1}):** 1602 ($\nu_{C=O}$ of pyrazolone), 1540 ($\nu_{C=O}$ of benzoyl), 1486 ($\nu_{C=N}$).

Complex-10: Pale bluish green crystal, yield: 83%, M.P:> 200°C, Molecular formula: $C_{40}H_{40}Cl_2NiN_4O_6S_2$, **M.W**: 802.37, Metal estimation, gravimetrically and volumetrically, **Elemental analysis**: C (Exp. 55.92%, Calc. 56.26%); H (Exp. 5.10%, Calc. 5.15%); N (Exp. 6.10%, Calc. 6.25%); Ni = 8.4%, **Molar conductance:** 2.20 $ohm^{-1}cm^2mol^{-1}$, **FTIR(KBr, cm^{-1}):** 1602 ($\nu_{C=O}$ of pyrazolone), 1540 ($\nu_{C=O}$ of benzoyl), 1486 ($\nu_{C=N}$).

5.2. Results and discussion

5.2.1. FTIR spectral studies

Table 5.1. FTIR spectral data of ligands and Ni(II) complexes

Code	$\nu_{C=O}$ of benzoyl chloride	$\nu_{C=O}$ of pyrazolone	Cyclic$\nu_{(C=N)}$	C–H in plane deformation	ν_{M-O}
HL^{VIII}	1606	1620	1400	1175	-
Complex-8	1558	1596	1486	1063	636

5.2.2. Thermogravimetric analysis

TGA, describes how the mass of a substance changes as a function of temperature. Thermal breakdown at temperatures between 100 and 550 °C serves as evidence of the remarkable thermal stability of the three synthesized Nickel(II) complexes.

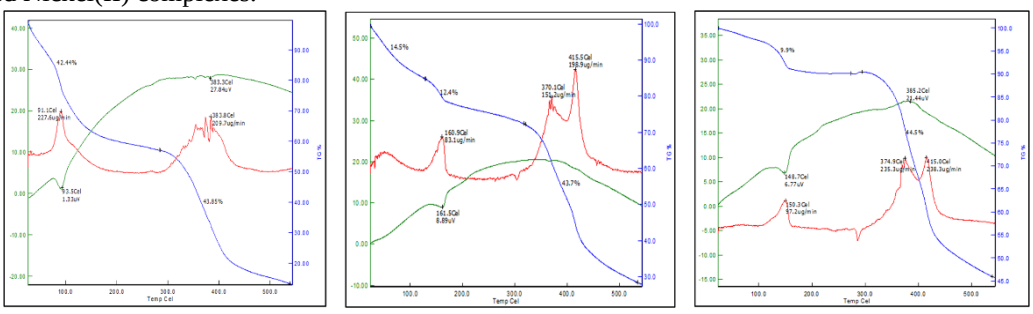

Fig.5.1. TG-DTA spectra of complex-8, complex-9 & complex-10 respectively

5.2.3. Single crystal X-ray diffraction study

The geometry of all the Ni(II) complexes is an octahedral which has been proved by single crystal X-ray diffraction analysis. The crystal of all three Ni(II) complexes is green, pale green and pale yellowish green

coloured respectively. The space group and crystal system of $[Ni(HL^{VIII})_2(EtOH)_2]$, $[Ni(HL^{IV})_2(DMF)(H_2O)]$, $[Ni(HL^{VI})_2(DMSO)_2]$ is $P\bar{1}$(Triclinic), $P\bar{1}$(Triclinic) and $P2_{1/n}$(Monoclinic) respectively.

α= 64.87(10)°	α= 65.19(2)°	α= 90°
β= 85.46(10)°	β= 76.26(2)°	β= 90.11(2)°
γ= 63.53(10)°	γ=84.90(2)°	γ=90°

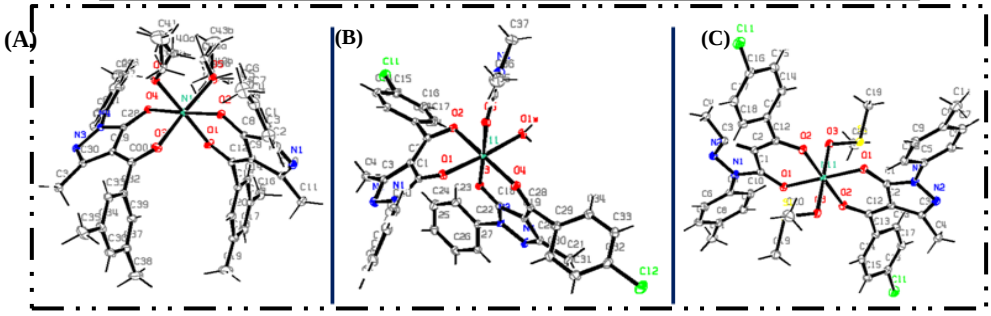

Fig.5.2. Unit cell dimensions & Thermal ellipsoid plots with a 50% probability (A)complex-8, (B)complex-9, (C)complex-10

5.2.3.1. Powder XRD analysis

. In the XRD graph, a sharp band is observed with maxima 2θ = 5 to 25° range for complex-10. The simulated pattern matches well with the experimental pattern which confirms a similar geometry of the complexes. This also ensures the structure obtained from a single crystal represents the bulk of the complexes.

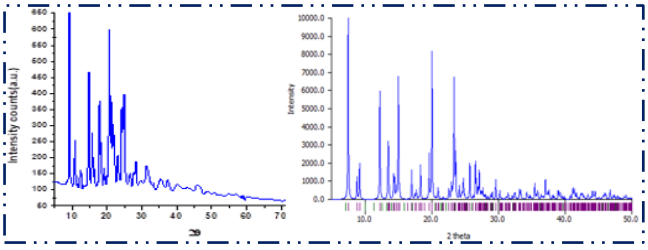

Fig.5.3. Experimental & Simulated powder XRD pattern of complex-10

5.2.4. DFT computational analysis

The geometry of all three Ni(II) complexes were optimized via B3LYP/LANL2DZ level basis set using Gauss View 6.0 software. The optimization energy is -105.7622 keV, -64.0523 keV and -66.3350 keV of complex-8,9,10 respectively. **Table 5.2. Global parameters of complex-10**

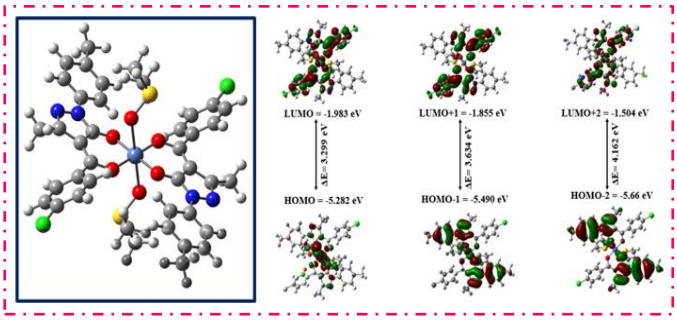

Fig.5.4. DFT optimized geometry & HOMO-LUMO diagram of complex-10

Properties	Mathematical Formula	Complex-10
Ionization potential (IP)	$IP = -E_{HOMO}$	5.282
Chemical Potential (μ)	$\mu = 1/2 (E_{HOMO} + E_{LUMO})$	-3.632
Softness (S)	$S = 1/2\eta$	0.303

5.2.5. 2D fingerprint combined with Hirshfeld surface analysis

The software CrystalExplorer17 was used to create the 2D fingerprint plots and Hirshfeld surface of the molecule, which also helped to show the structural links between the structural configurations of these closely related molecules. Short contact, donor-acceptor interaction sites and intermolecular interactions were analysed.

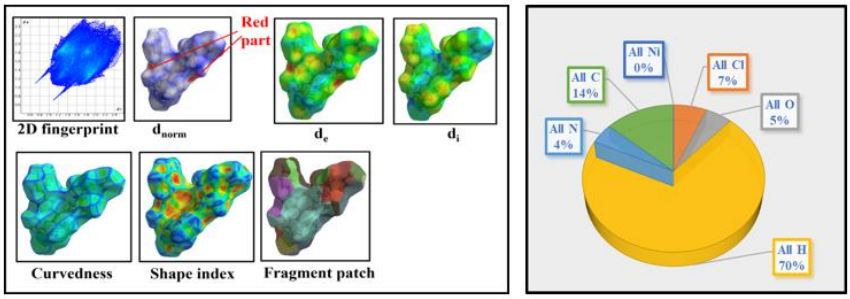

Fig.5.5. Molecular hirshfeld diagram of complex-10

5.2.6. Electronic spectral analysis

Electronic transition(d-d spectra) of NiL3A and NiL3 complexes were obtained in a 100% DMSO (1×10^{-3} M) solution up to 950 nm. While d-d bands of NiL1complex were obtained in 10^{-2} M concentration. Charge transfer (LMCT) spectra were recorded in a diluted solution of DMSO. Complex-8: π-π* transition (300 nm), n-π* transition (415 nm), Complex-9: π-π* transition (300 nm), n-π* transition (415 nm), Complex-10: π-π* transition (300 nm), n-π* transition (415 nm).

Table 5.3. Band Assignments of all three Ni(II) complexes

	Complex-8	Complex-9	Complex-10
$3A_{2g}\rightarrow3T_{1g}$(P)	516 nm, (1.7 $M^{-1}cm^{-1}$)	502 nm, (2.0 $M^{-1}cm^{-1}$)	773 nm, (0.3 $M^{-1}cm^{-1}$)
$3A_{2g}\rightarrow3T_{1g}$(F)	652 nm, (4.0 $M^{-1}cm^{-1}$)	669 nm, (3.8 $M^{-1}cm^{-1}$)	752 nm, (1.7 $M^{-1}cm^{-1}$)
$3A_{2g}\rightarrow3T_{2g}$	773 nm, (0.3 $M^{-1}cm^{-1}$)	652 nm, (3.0 $M^{-1}cm^{-1}$)	770 nm, (0.5 $M^{-1}cm^{-1}$)

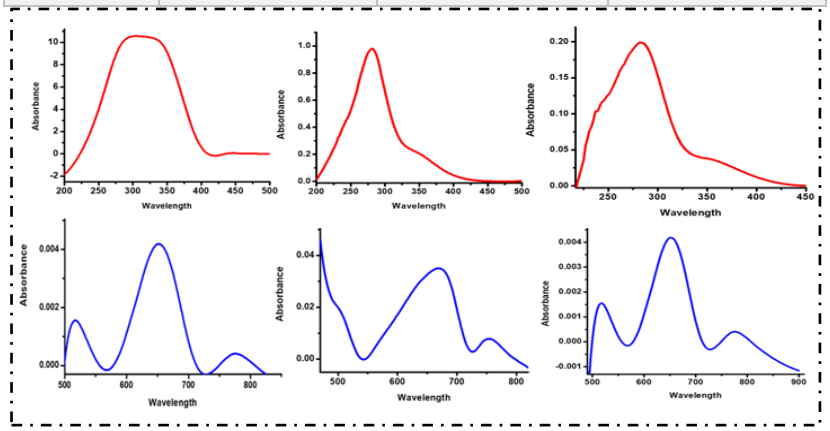

Fig.5.6. LMCT & d-d bands of (A)complex-8, (B)complex-9, (C)complex-10

5.2.7. Magnetic study

A superconducting quantum interference (SQUID) device is used to study a material's magnetic characteristics at different magnetic fields and temperatures. Temperature-dependent magnetisation data at 500 Oe(0.05T) was obtained using SQUID. According to Curie–Weiss paramagnetism, Magnetic susceptibility is inversely proportional to temperature hence, by increasing temperature the susceptibility decreases.

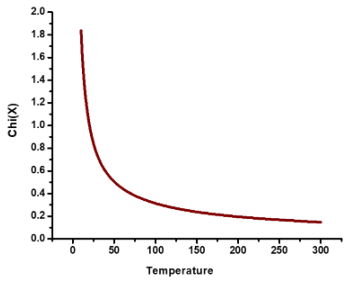

Fig.5.7. Appearance of Curie–Weiss behaviour in direct and inverse susceptibility

Conclusion

Acylpyrazolone based three Ni(II) complexes were synthesized having Octahedral geometry. All three complexes were characterized using analytical method. X-ray single-crystal diffraction data reveals that the ligand coupled

to Ni(II) ions in all three complexes via O donor atoms. Magnetic study revealed the paramagnetic nature of the complexes. Multiple interactions have been identified through Hirshfeld surface analysis. DFT and HOMO-LUMO study were conducted.

Publications from this research

[1] S. Barad, K. Chaudhari, R.N. Jadeja, H. Roy, D. Choquesillo-Lazarte, J. Mol. Struct. 1294 (2023) 136345.

[2] S. Barad, K. Chaudhari, H. Roy, R.J. Butcher, R.N. Jadeja, Inorganica Chim. Acta. 559 (2024) 121794.

[3] S. Barad, K. Chaudhari, R.N. Jadeja, H. Roy, R.J. Butcher, J. Coord. Chem. 76 (2023) 1955–1983.

[4] Sapna V. Barad, Rajendrasinh N. Jadeja, Ray J. Butcher, TMC (Manuscript ID: 9c55940f-7e33-45b3-bc2d-ab20b539b8ed v1.0) = Under Review

[5] Sapna V. Barad, Siddharth Saurabhb, Duane Choquesillo-Lazartec, R.N. Jadeja, JMS (MOLSTRUC-D-24-04267)

References

[1] N.U. N. UPADHAYAY, Synthesis, Characterization and Biological Studies of Some, Chem. Sci. Trans. 2 (2013) 455–460. https://doi.org/10.7598/cst2013.391.

[2] R.K. Sodhi, Metal Complexes in Medicine: An Overview and Update from Drug Design Perspective, Cancer Ther. Oncol. Int. J. 14 (2019). https://doi.org/10.19080/ctoij.2019.14.555883.

[3] M. Sekerci, F. Yakuphanoglu, Thermal analysis study of some transition metal complexes by TG and DSC methods, J. Therm. Anal. Calorim. 75 (2004) 189–195.https://doi.org/10.1023/B:JTAN.0000017341.20105.22.

[4] F. Marchetti, C. Pettinari, R. Pettinari, Acylpyrazolone ligands: Synthesis, structures, metal coordination chemistry and applications, Coord. Chem. Rev. 249 (2005) 2909–2945. https://doi.org/10.1016/j.ccr.2005.03.013.

[5] I. Shaikh, R.N. Jadeja, R. Patel, Three mixed ligand mononuclear Zn(II) complexes of 4-acyl pyrazolones: Synthesis, characterization, crystal study and anti-malarial activity, Polyhedron. 183 (2020) 114528. https://doi.org/10.1016/j.poly.2020.114528.

[6] B.S. Jensen, H. Meier, K. Lundquist, S. Refn, The Synthesis of 1-Phenyl-3-methyl-4-acyl-pyrazolones-5., Acta Chem. Scand. 13 (1959) 1668–1670. https://doi.org/10.3891/acta.chem.scand.13-1668.

[7] M. Travadi, R.N. Jadeja, R.J. Butcher, M.S. Shekhawat, Neodymium based acylpyrazolone complexes: Synthesis and physicochemical characterizations, Inorganica Chim. Acta. 559 (2024). https://doi.org/10.1016/j.ica.2023.121766.

•••

Barad Sapnaben Vishnubhai
Research Scholar

Dr. R. N. Jadeja
Research Supervisor

Department of Chemistry,
Faculty of Science,
The Maharaja Sayajirao University of Baroda
Vadodara.-390002. GUJARAT- INDIA.

Prof. Ashutosh V. Bedekar
Offg. Head
Department of Chemistry

HEAD
Department of Chemistry
Faculty of Science
The Maharaja Sayajirao University of Baroda
Vadodara - 390002. Gujarat - INDIA